Open Journal of Applied Sciences, 2019, 9, 68-86
http://www.scirp.org/journal/ojapps
ISSN Online: 2165-3925
ISSN Print: 2165-3917

Removal of Pertechnetate ($^{99}TcO_4^-$) from Liquid Waste by Magnesium Ferrite ($MgFe_2O_4$) Nanoparticles Synthesized Using Sol-Gel Auto Combustion Method

W. M. Abdellah[1*], A. Ezzat[2], I. Samir[3]

[1]Radiation Protection Department, Nuclear and Radiological Regulatory Authority, Cairo, Egypt
[2]Chemistry Department, Faculty of Science, Ain Shams University, Cairo, Egypt
[3]Central Laboratories, Nuclear and Radiological Regulatory Authority, Cairo, Egypt
Email: *wmsra@yahoo.com

How to cite this paper: Abdellah, W.M., Ezzat, A. and Samir, I. (2019) Removal of Pertechnetate ($^{99}TcO_4^-$) from Liquid Waste by Magnesium Ferrite ($MgFe_2O_4$) Nanoparticles Synthesized Using Sol-Gel Auto Combustion Method. *Open Journal of Applied Sciences*, **9**, 68-86.
https://doi.org/10.4236/ojapps.2019.92007

Received: January 8, 2019
Accepted: February 23, 2019
Published: February 26, 2019

Abstract

Low-cost adsorbents, Magnesium ferrite ($MgFe_2O_4$) nanoparticles were synthesized using three different types of fuel such as Urea, Oxalic acid, and Citric acid via sol-gel auto-combustion method. The prepared products were characterized by means of powder X-Ray Diffraction (XRD), Fourier Transform Infrared spectroscopy (FT-IR) and Field Emission Scanning Electron Microscope (FE-SEM). The influence of the fuel used on the morphology and the crystallite size of $MgFe_2O_4$ Nano products were studied. The results showed that Citric acid fuel produced pure $MgFe_2O_4$ with the smallest crystallite size average cluster = 13.53 nm. The synthesized sample was used for the removal of $^{99}TcO_4^-$ anions from low level liquid waste under studied conditions. The different parameters affecting on the adsorption process using the batch method were studied. The results revealed that $MgFe_2O_4$ nanostructure has high removal ability of $^{99}TcO_4^-$ from aqueous solutions (98.84%). The adsorption data are in good agreement with Freundlich and Pseudo second order isotherm models. The adsorption process was a chemisorption reaction additionally, the results of the thermodynamic parameters indicated that the adsorption of $^{99}TcO_4^-$ on nanostructures was an exothermic and spontaneous process.

Keywords

Magnesium Ferrite, Nanoparticles, Sol-Gel, Auto Combustion, Adsorption, Pertechnetate, Low Level Radioactive Waste

1. Introduction

Ferrites are ferromagnetic material containing predominantly iron oxides along with other oxides of barium, strontium, manganese, nickel, zinc, lithium and cadmium higher than 50%. The recycling of these materials and separating them using external magnet is applicable easily [1]. Previous studies indicate that spinel ferrite is a type of ferrites which has a formula MFe_2O_4 (M donates divalent cation as Mg^{2+}, Ni^{2+}, Zn^{2+}, Cd^{2+}, Mn^{2+} and Co^{2+}). Much attention and scientific interest have been paid to spinel ferrites as they have various chemical and physical properties for different applications in a wide range of technology. In particularly, $MgFe_2O_4$ is one of the spinel ferrite families of inverse spinel type; it has cubic structure and is a soft magnetic n-type semiconducting material [2]. Spinel ferrites are of great interest due to having diverse chemical and physical properties for various technological applications. In particularly, $MgFe_2O_4$ based materials have found applications in microwave devices, computer memory chips and high-density recording media [3]. $MgFe_2O_4$ based materials can be used as catalyst [4], inorganic pigment [5] [6], humidity sensor [7], gas sensor [8] [9], hyperthermia [10] [11], low magnetic materials [12] [13], semiconductors [14] [15], and anode material for lithium ion batteries [16]. Nano-Ferrites can be prepared using several techniques, such as polymeric precursors, micro emulsion, reverse micelle, hydrothermal, co-precipitation, sol-gel and solution combustion methods [2]. Sol-gel auto combustion synthesis is low annealing temperature, fast and effective method for producing fine and homogeneous Nano-sized ferrites with good chemical purity and improved physical properties [17]. The thermal and chemical stability of ferrite materials such as magnesium ferrite and its active sites plays an important role in the adsorption of various pollutants from aqueous media [18]. One of the most important pollutants is the radioactive isotopes such as technetium.

Technetium (^{99}Tc) is a pure beta emitter radionuclide that has a long half-life (2.13×10^5 years) with the maximum decay energy of 0.294 MeV and it causes a long-term radiation risk to humanity. A great attention shall be paid to ^{99}Tc during safety assessment of radioactivity in the environment, in decommissioning of nuclear facilities and management of nuclear waste as it has high mobility, high fission yield, and long half-life [19].

There diverse sources of ^{99}Tc such as fallout from nuclear weapons tests, discharges from nuclear power plants, nuclear medicine and radiobiology, resulted in raising the amount of ^{99}Tc released into the environment [19].

All of these activities generate large volumes of low and intermediate radioactive waste which can cause a significant impact on the environment if disposed without a suitable treatment. So, immobilization of long-lived radionuclides, such as ^{99}Tc into a relatively small volume waste is a vital for long term permanent disposal.

Um & Serne, in 2005 [20] studied the behavior of ^{99}Tc in the ground water and showed that it may be exist in the +III to +VII oxidation states under pH

and E_h values typical of most subsurface groundwaters, the dominant ^{99}Tc oxidation state in oxic ground waters is the highly mobile pertechnetate anion $[Tc(VII)O_4]^-$. Mobility of the pertechnetate anion is attributed to its inability to form stable aqueous complexes or solid phases under circumneutral-to basic pH conditions [20].

The objective of the present work is the synthesis of low-cost adsorbent like $MgFe_2O_4$ nanoparticles using sol-gel auto combustion method and study the effect of using different fuels such as Urea, Oxalic acid and Citric acid, moreover the effect of changing the calcination temperatures on the crystallite size and the morphology of the obtained products. The work has been extended to explore the possibility for the removal of pertechnetate, $^{99}TcO_4^-$ from a synthetic Low Level Radioactive Liquid Waste (LLRLW) by the prepared Nano-materials ($MgFe_2O_4$). The different parameters influencing on the adsorption process was performed in order to control the process along with examining the isotherm models, kinetics, and the thermodynamics of the reactions.

2. Experimental

2.1. Materials and Reagents

All chemicals were analytical grade, purchased and used as received without further purification: Magnesium nitrate $Mg(NO_3)_2 \cdot 6H_2O$ Merck; Ferric nitrate $Fe(NO_3)_2 \cdot 6H_2O$, Merck; Urea NH_2CONH_2; Fluka. Oxalic acid $C_2H_2O_4 \cdot 2H_2O$; Sigma-Aldrich; Citric acid $HOC(COOH)(CH_2COOH)_2$ Sigma-Aldrich; Ammonium hydroxide 25% NH_3 in H_2O, Sigma-Aldrich and $^{99}TcO_4^-$ radioactive waste was extracted from previously used ^{99m}Tc generator /columns collected from the nuclear medicine centers using diluted nitric acid.

2.2. Preparation of $MgFe_2O_4$ Nanostructures

Magnesium ferrite, $MgFe_2O_4$, nanostructures were synthesized via sol-gel auto combustion method [21] [22] [23] in which an aqueous solution of magnesium nitrate ($Mg(NO_3)_2 \cdot 6H_2O$) was added to a stirring aqueous solution of ferric nitrate ($Fe(NO_3)_2 \cdot 6H_2O$) and the reaction was heated up at 60˚C, and magnetically stirred for 10 min to the hot stirring solution an aqueous solution of Urea was added with molarity ratios between metal nitrate and the fuels (1:2). The solution was heated at 80˚C and stirred for one hour until the gel obtained. The produced solution was dried at 200˚C for 2 h. The produced foamy powder was ground and then, calcined at various temperatures 600˚C and 800˚C to give $MgFe_2O_4$ nanostructures referred as a_{600} and A_{800}, respectively. The produced magnesium ferrite samples (B and C) were prepared by applying similar conditions using Oxalic and Citric acids as a fuel, and the calcined products at 600˚C and 800˚C referred as (b_{600}, B_{800}) and (c_{600}, C_{800}) respectively. The synthesized samples were characterized for crystal phase identification by Powder X-Ray Diffraction (XRD) spectroscopy. The morphology was determined by the Field Emission Scanning Electron Microscopy (FE-SEM) and Fourier Transform

Infrared (FTIR) spectroscopy are recorded using KBr pellets on a BRUKER® Tensor 27 FT-IR spectrometer, in the range of 4000 - 400 cm^{-1}.

2.3. Adsorption Studies

Batch experiments were carried out to examine the sorption of pertechnetate, $^{99}TcO_4^-$ from aqueous solution by the synthesized Nano $MgFe_2O_4$. For the sorption determination, a certain weight (50 mg) of the investigated material ($MgFe_2O_4$) contacted with 10 ml of solution contain $^{99}TcO_4^-$ at different activity concentration from 2.13 to 15.58 Bq/vial for 24 hours. The sample suspensions were shaken at room temperature (25˚C), then centrifuged at 4000 rpm for 10 minutes. The activity concentration of the obtained solution was determined by Liquid Scintillation Counter (LSC) (type: Packard, USA, model 3720) by mixing 5 ml of the supernatant with 5 ml of ultima gold liquid scintillation cocktail and feeding the measuring vials to the Liquid Scintillation Counter (LSC). The adsorption capacity of the adsorbent (q_t, Bq/g); was calculated from Equation (1) [24], where, C_0 is the initial $^{99}TcO_4^-$ concentration, C_t is the $^{99}TcO_4^-$ concentration in solution at a pre-defined time t, V (L) is the volume of the $^{99}TcO_4^-$ solution, and m (g) is the mass of $MgFe_2O_4$ adsorbent. Moreover, Equation (2) [24] was employed to estimate the removal percent (%R) of the $^{99}TcO_4^-$.

$$q_t = (C_0 - C_t) \times \frac{V}{m} \tag{1}$$

$$^{99}TcO_4^- R\% = \frac{C_0 - C_t}{C_0} \times 100 \tag{2}$$

Various factors have been investigated such as contact time (20 - 120 min), pH (2 - 9), competing cation concentration KCl (0.05 - 0.55 g), temperature (25˚C - 55˚C), and initial $^{99}TcO_4^-$ activity concentration of 951 CPM/vial (3.17 Bq/ml). The equilibrium adsorption capacity of $MgFe_2O_4$ adsorbent, q_e (Bq/g) can be determined from Equation (3).

$$q_e = (C_0 - C_e) \times \frac{V}{m} \tag{3}$$

where: C_e (Bq/l) is the $^{99}TcO_4^-$ concentration at equilibrium in the supernatant after separation of the adsorbent and V, m, and C_0 have the same meaning as in Equations (1) and (2).

3. Results and Discussion

3.1. Structural Characterization

X-Ray Diffraction

The XRD patterns of magnesium ferrite samples produced by calcination of the combusted precursors at 600 and 800˚C are shown in **Figures 1(a)-(c)** and **Figures 2(a)-(c)**, respectively. It is clearly observed that the calcination temperature 600˚C was not enough to produce a pure phase of $MgFe_2O_4$ with samples (a) and (b) as in **Figure 1** which prepared using Urea and Oxalic acid as fuels

respectively. The sample (a) showed a characteristic peak of hematite at 2θ = 35.48 corresponding to (JCPDS File No. 79-1741). The pattern sample (b) has some intermediate products of Magnesium oxide and hematite that evidenced from their reflection patterns at (2θ = 78.74, 2θ = 74.70) indexed to (JCPDS File No. 87-0652) and at (2θ = 33.11, 2θ = 49.41) indexed to (JCPDS File No. 89-0598), respectively. A similar approach is used for sample (c) **Figure 1** revealed the production of single phase of magnesium ferrite with a relatively low amount of impurities.

The diffraction peaks of samples (a) and (c) were consistent very well with the cubic $MgFe_2O_4$ with cell parameters; a = 8.386 Å and V_{cell} = 589.81 Å^3 (JCPDS File No. 088-1937). But for sample (b), when oxalic acid is used as a fuel, the diffraction peaks of sample (b) was indexed well with the cubic $MgFe_2O_4$ with cell parameters; a = 8.380 Å and V_{cell} = 588.61 Å^3 (JCPDS File No. 088-1935). The same results of getting impure phase with urea fuel and obtaining pure phase with citric acid fuel was reported by Druc *et al.* in 2013 [25]. On the other hand, the calcination temperature for the three samples was raised to 800˚C to investigate its effect on the phase composition of the combustion products of the three fuels. **Figures 2(a)-(c)** shows the XRD patterns of the produced magnesium ferrite samples by calcination of the ignited products at 800˚C, it is obvious from **Figure 2** that the calcination temperature at 800˚C was enough to produce a crystalline single product with the three fuels and all the diffraction peaks in **Figure 2** are consistent well the cubic $MgFe_2O_4$ (JCPDS File No. 088-1937). Moreover, the crystallite size (D, nm) of magnesium ferrite products was calculated using the Debye-Scherer Equation (4) [26].

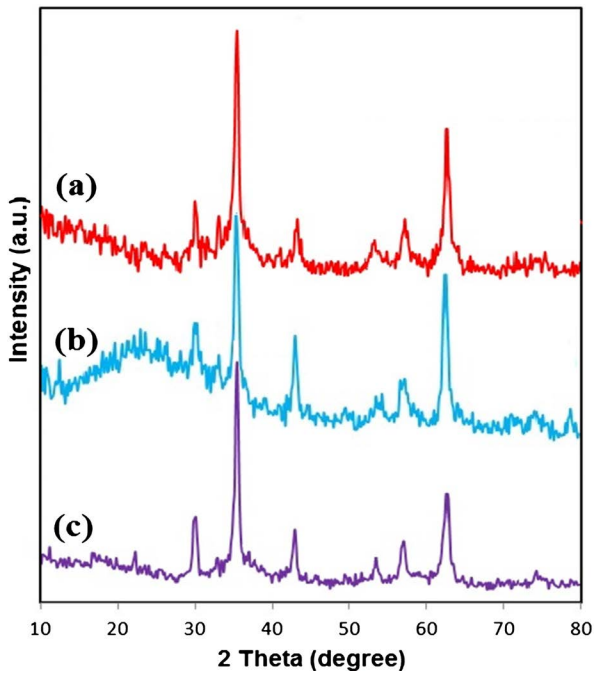

Figure 1. XRD patterns of $MgFe_2O_4$ samples calcined at 600˚C prepared by Urea (a), Oxalic acid (b) or Citric acid (c).

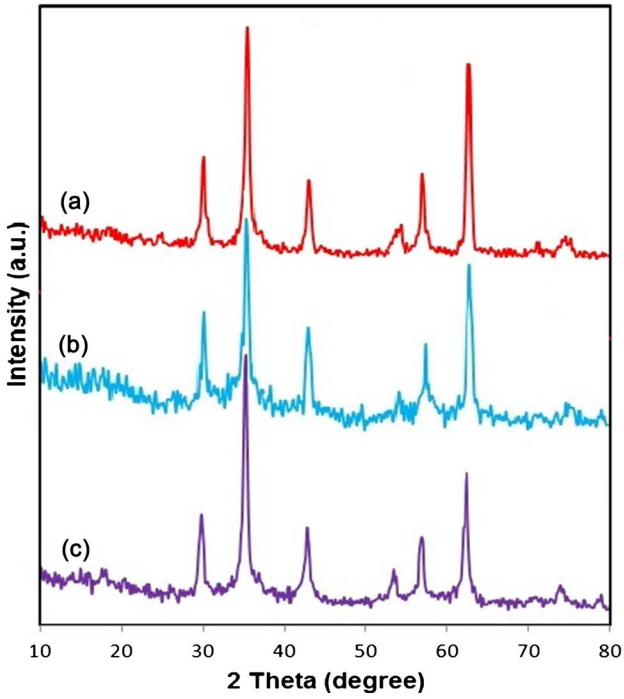

Figure 2. XRD patterns of $MgFe_2O_4$ samples calcined at 800˚C prepared by Urea (a), Oxalic acid (b) or Citric acid (c).

$$D = \frac{0.9\lambda}{\beta \cos \theta B} \tag{4}$$

where, λ (nm) is the X-ray radiation wavelength, β is the diffraction peak full width at half maximum (FWHM), and θB is the Bragg diffraction angle. The average crystallite size of the prepared $MgFe_2O_4$ nanoparticles calcined at 600˚C was about 10.41, 15.15 and 13.53 nm for samples a_{600}, b_{600} and c_{600} respectively. Additionally, the crystallite size was increased to 18.88, 18.56 and 15.22 nm on increasing the calcination temperature to 800˚C for samples A_{800}, B_{800} and C_{800} respectively. It can be concluded that, changing of the used fuel has a remarkable effect on both the particle size and the phase of the synthesized Nano-$MgFe_2O_4$, since using the citric acid fuel produced pure $MgFe_2O_4$ nanostructure with the smallest crystallite size at lower temperature (600˚C). Therefore, Citric acid is the optimum fuel in the present work.

FT-IR Analysis Nanoparticles

FT-IR spectroscopy is one of the most important and widely used analytical methods for obtaining information about the presence of certain functional groups in the structure of the magnetic nanomaterials. **Figure 3** shows FT-IR spectra (A-C) for samples A_{800}, B_{800}, and C_{800} prepared by Urea, Oxalic acid and Citric acid as a fuel respectively and annealed at 800˚C. The IR spectra of the samples showed a strong absorption band at 567, 563 and 568 cm^{-1} for sample A, B, and C, respectively, which is characteristic and indicates the formation of $MgFe_2O_4$.

In ferrites crystal structure the metal ions have two characteristic different sub

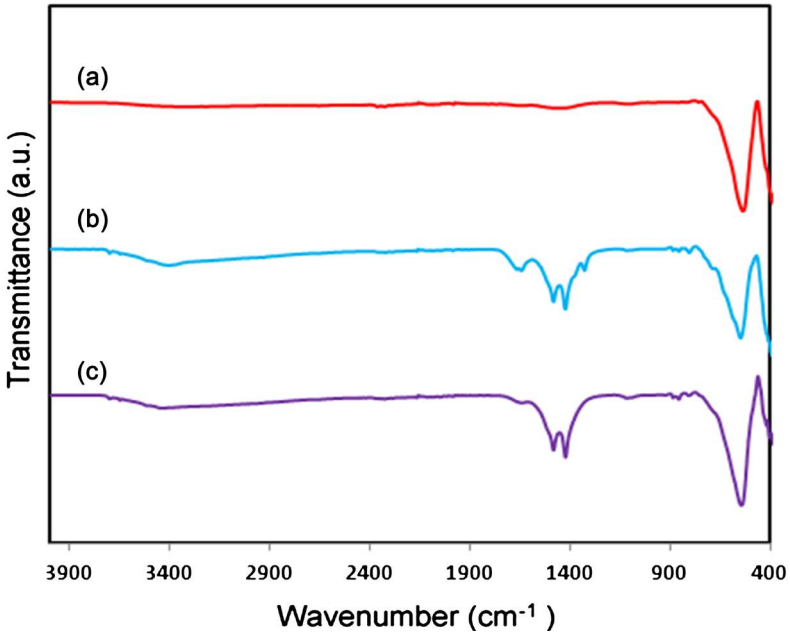

Figure 3. FT-IR spectra of $MgFe_2O_4$ products calcined at 800˚C prepared by Urea (a), Oxalic acid (b) or Citric acid (c).

lattices, known as tetrahedral and octahedral according to the geometrical configuration of the oxygen nearest neighbors. The metal-oxygen band at 567, 563 and 568 cm^{-1} corresponds to the intrinsic stretching vibrations of the metal at the tetrahedral site [27]. Sample B_{800} shows a weak absorption band at 1336 cm^{-1} that is related to carbonate ions [27]. The band at wavenumber 1425 and 1421 for samples B_{800} and C_{800} respectively is a characteristic absorption peak for CO_3^{2-}. However, the IR spectra also showed abroad vibration band at 3421 and 3434 cm^{-1} for the B_{800}, and C_{800} samples, respectively, that can be assigned to the OH stretching vibrations of water molecules (physical adsorbed molecular water) while their bending mode appeared at 1641and 1635 cm^{-1} for the B_{800}, and C_{800} respectively [28].

Field Emission Scanning Electron Microscopy (*FE-SEM*) *of $MgFe_2O_4$ Nanoparticles*

Magnesium ferrite $MgFe_2O_4$ nano-structures were observed using a scanning electron microscope are shown in **Figures 4(a)-(c)**, which denoted as a_{800}, b_{800} and c_{800} referred to the used fuels Urea, Oxalic acid and Citric acid respectively in the preparation process. It is observed that the micrograph of sample (a_{800}) in **Figure 4** shows aggregates of wool or cotton of the spherical with average crystallite size about 20 μm. On the other hand, **Figure 4(b)** & **Figure 4(c)** revealed that the products (b_{800} and c_{800}) are composed of small single spheres, bulk agglomerates of sphere like structures and foamy structures with average size of 20 μm. The image illustrated that the spheres in the micrograph of sample b_{800} are relatively smaller than that in sample c_{800}. The aggregates in the SEM images of the three samples could be attributed to the interaction between the nanoparticles due to the magnetic nature of the $MgFe_2O_4$ samples. In cases of nanocrystalline

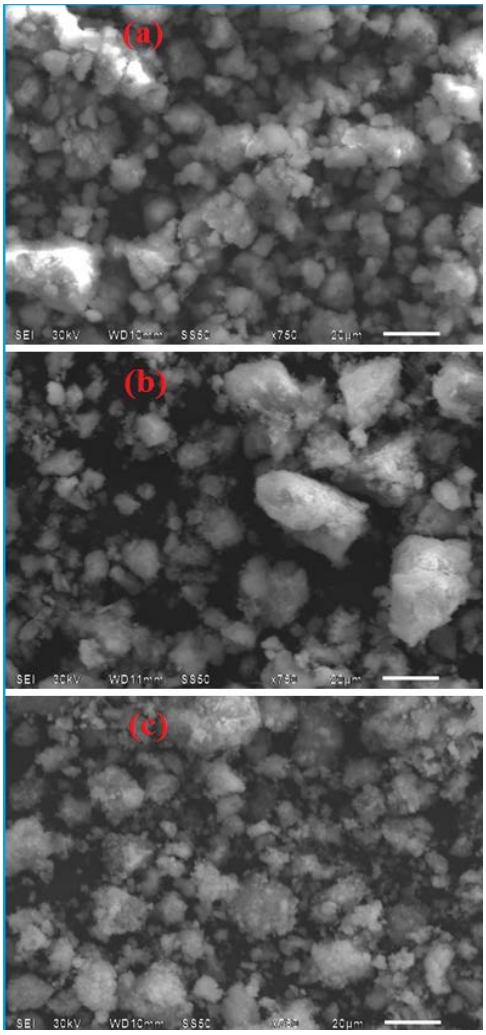

Figure 4. FE-SEM image of $MgFe_2O_4$ products calcined at 800˚C prepared by Urea (a), Oxalic acid (b) or Citric acid (c) as a fuel.

spinel ferrites, it has been observed that there is a tendency for the nanoparticles to agglomerate as reported by Naseri *et al.*, in 2014 [29]. From obtained results it can be concluded that the fuel type in the combustion process could affect the morphology of the final product.

3.2. Batch Adsorption Experiment

Effect of solution pH

The influence of the initial pH of the solution on the removal percent of the investigated isotope ($^{99}TcO_4^-$) was investigated in the pH range from 2 to 9 (**Figure 5**). The experimental data revealed that the removal percentage of $^{99}TcO_4^-$ is high at low pH values, it reaches the maximum removal% at pH ~2 (%R = 99.02%) followed by a plateaued over a wide pH range from pH 3 to 7 (%R = 98.69% - 98.59%), Afterward, the removal percentage reduces sharply for $^{99}TcO_4^-$ on increasing the pH values to 9. The behavior can be explained by considering the surface charge of the $MgFe_2O_4$ nanoparticles and the $^{99}TcO_4^-$

anions at different pH values. At lower pH values, the $MgFe_2O_4$ adsorbent surfaces (hydrous oxide (MOH)) will be probably covered by protons forming positively charged particles MOH^{+2}. However, at higher pH values, hydroxide ions are available in high concentrations and may react with the hydrous oxide forming negatively charged deprotonated oxide (MO^-) [25] [30]. The adsorption process may be controlled by the electrostatic interactions between the negatively charged pertechnetate anions and the positively charged $MgFe_2O_4$ adsorbent. This behavior enhancing the adsorption process at lower pH values, but the adsorption efficiency percent decreased at higher pH values due to the competition between the high concentrations of OH^- ions and the negatively charged $^{99}TcO_4^-$ anions [31].

Effect of contact time

The influence of contact time on the adsorption efficiency of $^{99}TcO_4^-$ anions by $MgFe_2O_4$ nano-adsorbent was studied using 0.05 g $MgFe_2O_4$ Nano-adsorbent and initial concentration of 128 CPM/vial to 951 CPM/vial (0.43 Bq/ml to 3.17 Bq/ml) for $^{99}TcO_4^-$. **Figure 6** represents the $^{99}TcO_4^-$ removal percentage against shaking time ranged from 20 to 120 min. The sorption of the investigated isotope $^{99}TcO_4^-$ increases with time to reach a saturation level 98.84% for 100 min. depending on the nature of the isotope and selectivity of the prepared Nano adsorbent. The instantaneous removal percent of the investigated isotope by $MgFe_2O_4$ indicates that the mechanism of the sorption may be ion exchange [32].

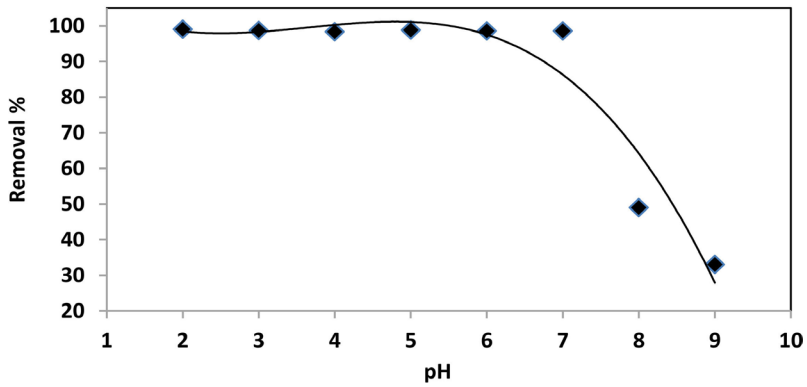

Figure 5. Effect of pH on $^{99}TcO_4^-$ removal percent using $MgFe_2O_4$ nano-adsorbent.

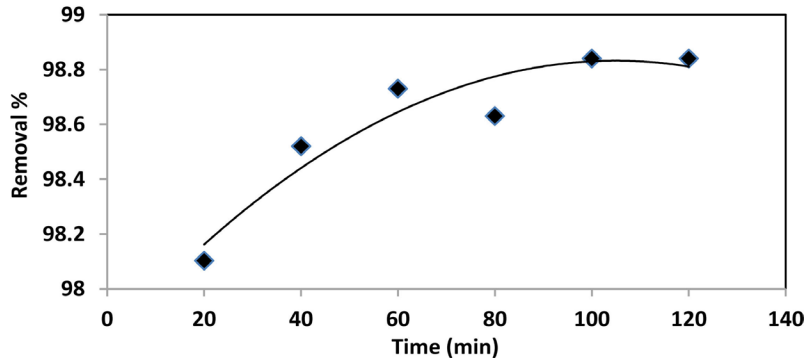

Figure 6. Effect of contact time on $^{99}TcO_4^-$ removal percent using $MgFe_2O_4$ nano-adsorbent.

Effect of temperature

The effect of different temperature (25˚C, 35˚C, 45˚C and 55˚C) on the adsorption of $^{99}TcO_4^-$ was investigated at initial concentration of 951 CPM/vial (3.17 Bq/ml) for $^{99}TcO_4^-$.and 0.05 g from the nano-$MgFe_2O_4$ **Figure 7**, shows a relatively decrease in the removal percentages of $^{99}TcO_4^-$ on $MgFe_2O_4$ this may be attributed to the increasing mobility of $^{99}TcO_4^-$ ions as the temperature increases, causing small amounts of the ions escapes from the solid phase to the liquid phase [27]. This in turn, means that the reaction may be has an exothermic nature and the adsorption process is favored at low temperatures.

Effect of competing ion concentration

The effect of ionic strength on the adsorption of $^{99}TcO_4^-$ on $MgFe_2O_4$ was investigated utilizing KCl salt at different weight from 0.05 to 0.55 g. The results shown in **Figure 8** reveal that, the solution ionic strength has a negative effect on $^{99}TcO_4^-$ ions removal percentage, as increasing the ionic strength decreases the $^{99}TcO_4^-$ ions adsorption percentage. The significant decrease of removal percentage may be due to the competition between the $^{99}TcO_4^-$ ions and chloride ions in the solution. In other words, as a result of the electrostatic attraction between the negatively charged $^{99}TcO_4^-$ ions and the positively charged $MgFe_2O_4$

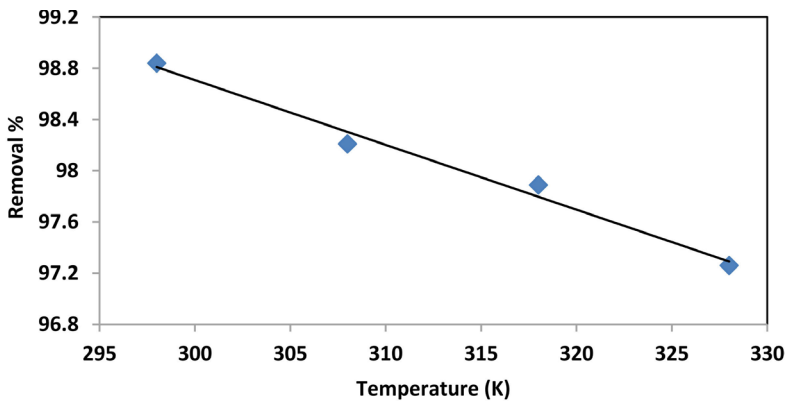

Figure 7. Effect of temperature on $^{99}TcO_4^-$ removal percent using $MgFe_2O_4$ nano-adsorbent.

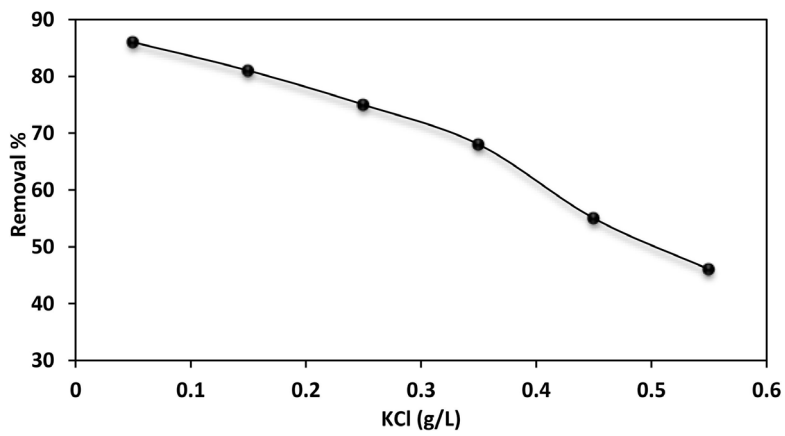

Figure 8. Effect of KCl concentration on $^{99}TcO_4^-$ removal percent using $MgFe_2O_4$ nano-adsorbent.

adsorbent surface, the increase in the solution ionic strength will result in a reduction of the adsorption capacity and this agree with the investigators Ali *et al.*, in 2016 [33] and Reddad *et al.*, in 2002 [34].

Effect of initial $^{99}TcO_4^-$ *activity concentration*

$^{99}TcO_4^-$ activity concentration ranged from 128 CPM/vial to 951 CPM/vial (0.43 Bq/ml to 3.17 Bq/ml) and utilizing 0.05 g $MgFe_2O_4$ as adsorbent. The adsorption capacity increased with increasing the initial activity concentration for $^{99}TcO_4^-$ and it reached 186.4 CPM/g (3.11 Bq/g) corresponding to activity 951 CPM/vial (3.17 Bq/ml) (**Figure 9**). This behavior could be assigned to the higher driving force at more $^{99}TcO_4^-$ ions that ease the diffusion of the ions from the solution to the positively charged $MgFe_2O_4$ nanoparticles surfaces, and hence more interactions between $^{99}TcO_4^-$ ions and the active sites of $MgFe_2O_4$ sorbent [35].

3.3. Adsorption Isotherms

Adsorption isotherm is the relationship at equilibrium between the quantity of adsorbate per unit of adsorbent (q_e) and its equilibrium solution concentration (C_e) at a constant temperature. To determine the adsorption capacity of the $MgFe_2O_4$ nanoparticles, the equilibrium data for the adsorption of $^{99}TcO_4^-$ on $MgFe_2O_4$ nanoparticles are analyzed in the light of Langmuir and Freundlich adsorption isotherm models [36] [37].

Langmuir isotherm model

Formation of a monolayer adsorbate on the outer surface of the adsorbent, and no further adsorption takes place again, is the assumption of Langmuir isotherm model. It is applicable for monolayer adsorption onto adsorbent surface that has a finite number of identical sites and no transmigration of adsorbate in the plane of the surface. According to these assumptions, the linear equation of Langmuir isotherm model can be written as follows [36].

$$\frac{C_e}{q_e} = \frac{1}{Q_0 b} + \frac{C_e}{Q_0} \tag{5}$$

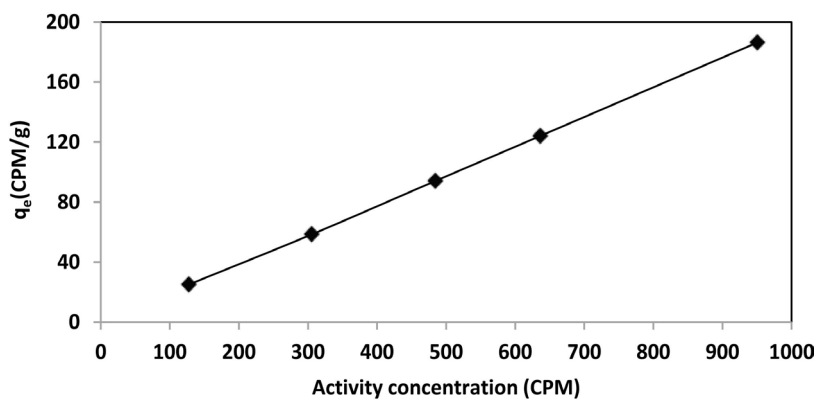

Figure 9. Effect of initial $^{99}TcO_4^-$ concentration on the adsorption capacity of $MgFe_2O_4$ nano-adsorbent.

where: C_e is the concentration of $^{99}TcO_4^-$ anions solution (CPM/l) at equilibrium, the constant Q_0 refers to the adsorption capacity (CPM/g) and b, Langmuir constant that is related to the energy of adsorption. Linear plot of C_e/q_e versus C_e shows Langmuir isotherm (Figure 10). Values of Q_0 and b were calculated from the slope and intercept of the linear plots and are presented in Table 1. Moreover, the equilibrium parameter R_L which is characteristic of Langmuir isotherm can be, defined as:

$$R_L = \frac{1}{1 + bC_0} \tag{6}$$

where: b is the Langmuir constant and C_0 is the initial $^{99}TcO_4^-$ concentration CPM/vial or (Bq/ml), R_L value indicates the adsorption nature to be either favorable if $0 < R_L < 1$, linear if $R_L = 1$, unfavorable if $R_L > 1$ and irreversible if $R_L = 0$ [38]. Table 1 shows R_L values between zero and one, which indicate favorable adsorption process.

Freundlich isotherm model:

Freundlich isotherm model assumes that the adsorption takes place on a heterogeneous surface of the adsorbent and the linearized form of this model can be given by Equation (7) [37].

$$\ln q_e = \ln K_f + (1/n) \ln C_e \tag{7}$$

where: K_f is the Freundlich constant (CPM/g) which represents the relative adsorption capacity of the adsorbent. $(1/n)$ is the heterogeneity factor and it is a function of the strength of adsorption in the adsorption process and n has various values depending on the heterogeneity of the sorbent. If n lies between one and ten, this indicate a favorable sorption process [39]. $1/n$ and $\ln K_f$ values were calculated from the slope and intercept of the linear plots of $\ln q_e$ versus $\ln C_e$ which shows Freundlich isotherm (Figure 11) and are presented in Table 1.

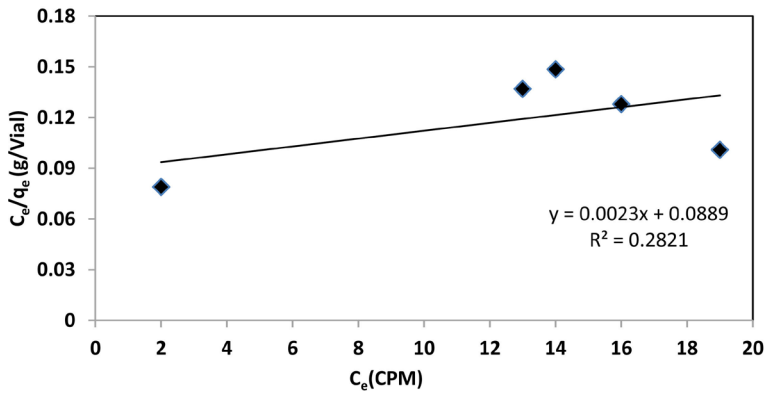

Figure 10. Langmuir isotherm for adsorption of $^{99}TcO_4^-$ on $MgFe_2O_4$ nano-adsorbent.

Table 1. Langmuir and Freundlich constants and R^2 values obtained for removal of $^{99}TcO_4^-$ by $MgFe_2O_4$ nano-particles.

Pollutant	Langmuir			Freundlich		
	q_o (CPM/g)	R_L	R^2	$1/n$	K_F	R^2
$^{99}TcO_4^-$	434	0.040	0.282	0.793	13.88	0.948

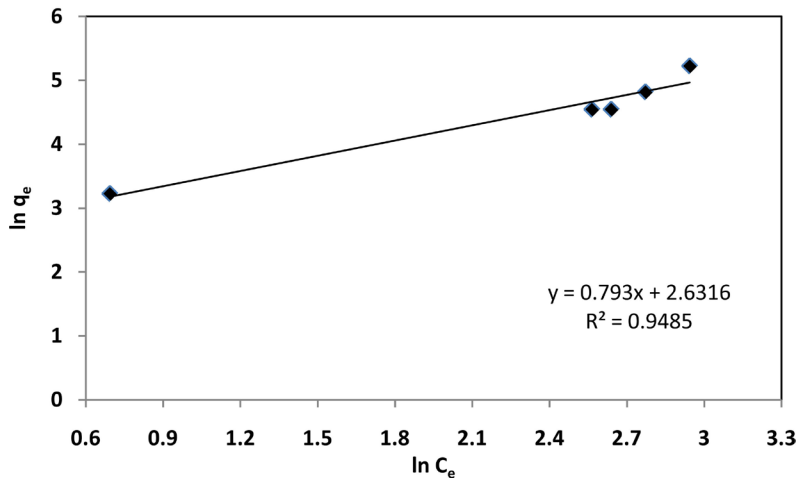

Figure 11. Freundlich isotherm for adsorption of $^{99}TcO_4^-$ on $MgFe_2O_4$ nano-adsorbent.

From **Table 1**, it is observed that, the heterogeneity parameter, $1/n$, for $^{99}TcO_4^-$ ($1/n = 0.793$, $n = 1.261$), which indicates a favorable sorption process as (n) lies between one and ten [39]. Moreover, the correlation coefficient (R^2) values of Freundlich isotherm for $^{99}TcO_4^-$ is closer to unity and greater than that in Langmuir isotherm, So, we conclude that the adsorption of $^{99}TcO_4^-$ by $MgFe_2O_4$ as adsorbent fits Freundlich isotherm model and this in turn suggests that the adsorption process occurs as a multilayer $^{99}TcO_4^-$ molecules adsorb onto the heterogeneous adsorbent surface.

3.4. Kinetics Adsorption Models

Pseudo first and second order reaction rate models were used to describe the adsorption behavior of the reaction at which the $^{99}TcO_4^-$ anions is removed from aqueous solutions. Pseudo first order rate equation of Lagergen is given by Equation (8) [40].

$$\log(q_e - q_t) = \log q_e - (K_{1,ads}/2.303)t \tag{8}$$

where: q_e and q_t are the amounts of $^{99}TcO_4^-$ anions adsorbed (CPM/g) at equilibrium and at time t (min), respectively and $K_{1,ads}$ is the rate constant of pseudo first order adsorption (min^{-1}). Values of $K_{1,ads}$ were calculated from the plots of $\log(q_e - q_t)$ versus t (**Figure 12**).The rate equation for pseudo-second order model is given by equation (9) [41].

$$t/q_t = 1/(k_{2,ads}q_e^2) + (1/q_e)t \tag{9}$$

where: $k_{2,ads}$ (g/CPM min) is the pseudo second order rate constant and its value was obtained from the plots of t/q_t versus t (**Figure 13**). **Table 2** lists the rate constants, calculated equilibrium adsorption capacity q_e(cal) and experimental equilibrium adsorption capacity q_e(exp) for $^{99}TcO_4^-$ obtained using the pseudo-first and second order models. It is obvious that q_e value calculated from pseudo first order kinetic model was too small compared to the experimental value for $^{99}TcO_4^-$ anions. However, the calculated q_e from pseudo second order

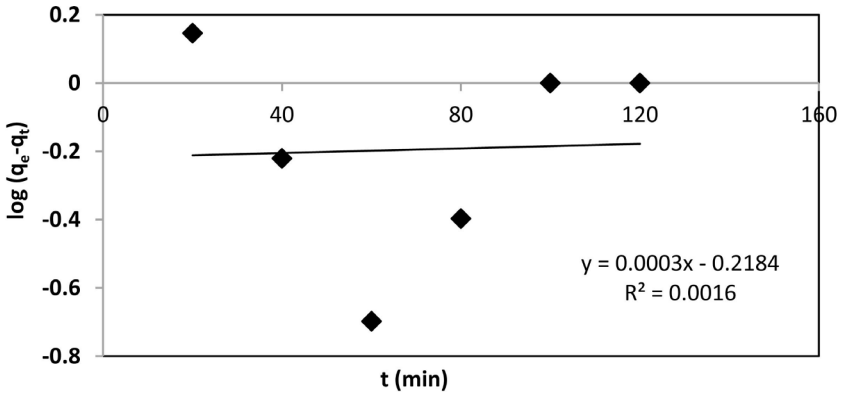

Figure 12. Pseudo-first-order plots for adsorption of $^{99}TcO_4^-$ on $MgFe_2O_4$ nano-adsorbent.

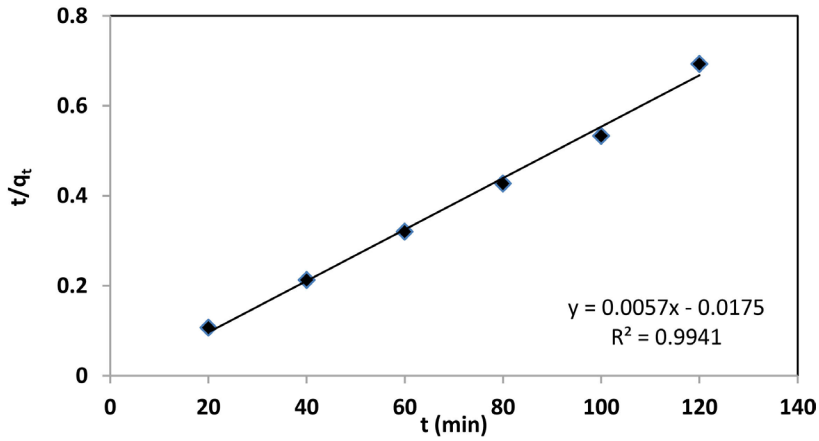

Figure 13. Pseudo-second-order plots for adsorption of $^{99}TcO_4^-$ on $MgFe_2O_4$ nano-adsorbent.

Table 2. Pseudo first and second order reaction rate models' parameters for adsorption.

Pollutant	Pseudo first order kinetic				Pseudo second order kinetic			
	k_1 (1/min)	$q_{e(cal)}$ (CPM/g)	$q_{e(exp)}$ (CPM/g)	R^2	k_2 (g/CPM.min)	$q_{e(cal)}$ (CPM/g)	$q_{e(exp)}$ (CPM/g)	R^2
$^{99}TcO_4^-$	0.0006	187.6	0.604	0.0016	0.001	187.6	175.438	0.99

kinetic model was relatively close to the experimental value. Additionally, the correlation coefficient (R^2) values of pseudo second order model is closer to unity. These results show that the pseudo second order adsorption mechanism is predominant and adsorption process of $^{99}TcO_4^-$ anions appeared to controlled by the chemisorption process. $^{99}TcO_4^-$ anions can be ionized in solution to form negative ions and the nano-$MgFe_2O_4$ carry a positive charge, which may lead to a chemical reaction through electrostatic interaction between a positive charge at the surface of $MgFe_2O_4$ nanoparticles and the negative charge on pertechnetate anions [42].

3.5. Thermodynamic Studies for Adsorption $^{99}TcO_4^-$ on $MgFe_2O_4$

Van't Hoff Equation (10), was used to calculate the thermodynamic parameters such as change in enthalpy (ΔH^o), change in entropy (ΔS^o) and change in free

energy (ΔG^{o}). Adsorption of $^{99}TcO_4^-$ on $MgFe_2O_4$, at different temperatures were determined by using Equations (11) & (12) and illustrated in Figure 14. The values of ΔH^{o} and ΔS^{o} were calculated from Figure 14 and reported in Table 3.

$$\ln K_d = \frac{\Delta S^\circ}{RT} - \frac{\Delta H^\circ}{RT} \tag{10}$$

$$K_d = \frac{C_{Ae}}{C_e} \tag{11}$$

$$\Delta G^\circ = \Delta H^\circ - T\Delta S^\circ \tag{12}$$

where: K_d is the equilibrium constant, C_{Ae} is the solid phase concentration at equilibrium (mg/L), T is the temperature in kelvin and R is the gas constant. Plotting $\ln K_d$ against $1/T$ gives a straight line with slope and intercept equal to—$\Delta H^{o}/R$ and $\Delta S^{o}/R$, respectively. The values of ΔH^{o} and ΔS^{o} were calculated from Figure 14 and reported in Table 3. The negative values of ΔH^{o} indicate the exothermic nature of adsorption process. The negative value of entropy change (ΔS^{o}) corresponds to a decrease in degree of freedom of the adsorbed species. This suggests the decrease in concentration of adsorbate in solid solution interface indicating an increase in adsorbate concentration on the solid phase. This is the

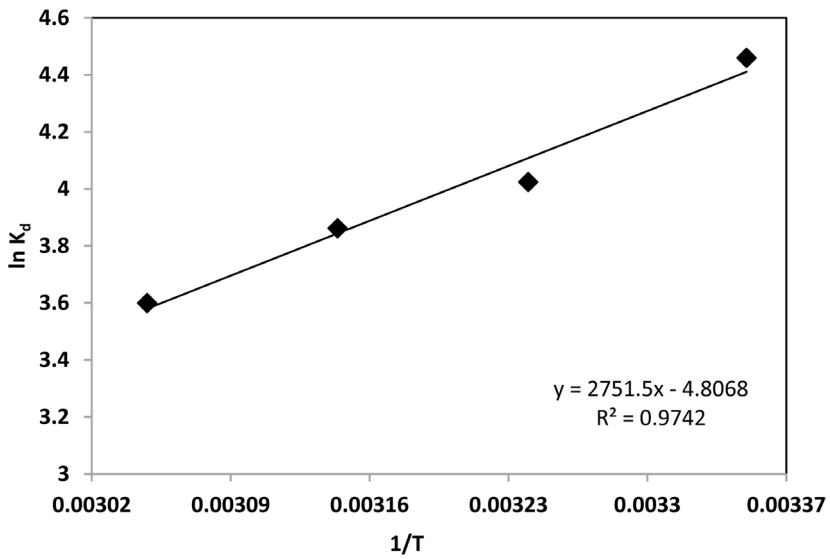

Figure 14. Van't Hoff plot for adsorption of $^{99}TcO_4^-$ on $MgFe_2O_4$ nano-adsorbent.

Table 3. Thermodynamic parameters for adsorption of $^{99}TcO_4^-$ on $MgFe_2O_4$ nanoparticles.

Temp (K)	ΔG^{o} (kJ/mol)	K_d	ΔH^{o} (kJ/mol)	ΔS^{o} (J/mol K)
298	−11.047	86.45		
308	−10.304	55.94		
			-22.87	-0.039
318	−10.207	47.55		
328	−9.814	36.57		

normal effect of chemical adsorption phenomenon, which takes place through electrostatic attraction. Gibbs free energy of adsorption (ΔG^o) was calculated from Equation (12) and the values are given in **Table 3**. The negative value of ΔG^o indicates that the adsorption of $^{99}TcO_4^-$ on Nano-magnesium ferrite is a spontaneous process, whereby no energy input from outside of the system is required. However, the values of ΔG^o decreased with increasing of temperature suggesting that adsorption became less favorable at higher temperatures. As the temperature increases, the mobility of $^{99}TcO_4^-$ anions increases, causing the anions to escape from the solid phase to the liquid phase. Therefore, the amount of $^{99}TcO_4^-$ anions that can be adsorbed will decrease. The increased mobility of $^{99}TcO_4^-$ anions at elevated temperature may be reflected in the values of K_d (**Table 3**). As the temperature increased the values of K_d decreased indicating a lower affinity of the $MgFe_2O_4$ nanoparticles towards $^{99}TcO_4^-$ anions at higher temperatures [43] [44].

4. Conclusion

Low cost adsorbent $MgFe_2O_4$ nanoparticles were prepared successfully. The prepared pure phase produced by using citric acid as a fuel was tested for the removal of $^{99}TcO_4^-$ anions from low level liquid waste and showed high removal percentage reached 98.84% within equilibrium time 100 minutes. The removal efficiency was decreased with increasing the added KCl dose. The rate of the reaction is pseudo second order with R^2 (0.99). The reaction followed Freundlich isotherm model with R^2 (0.95) which indicated to chemisorption process. The negative value of enthalpy (ΔH^o) indicates the exothermic nature of the reaction, and the negative value of the change in free energy (ΔG^o) illustrates that the adsorption of $^{99}TcO_4^-$ anions on Nano-$MgFe_2O_4$ is a spontaneous process. Finally, it can be concluded that $MgFe_2O_4$ nanoparticles are an efficient adsorbent for removal of $^{99}TcO_4^-$ anions from low level radioactive liquid waste.

Conflicts of Interest

The authors declare no conflicts of interest regarding the publication of this paper.

References

[1] Singhal, S., Sharma, R., Singh, C. and Bansal, A.S. (2013) Enhanced Photocatalytic Degradation of Methylene Blue Using $ZnFe_2O_4$/MWCNT Composite Synthesized by Hydrothermal Method. *Indian Journal of Materials Science*, **1**, Article ID: 356025. https://doi.org/10.1155/2013/356025

[2] Feng, Y., Li, S., Zheng, Y., Yi, Z., He, Y. and Xu, Y. (2017) Preparation and Characterization of $MgFe_2O_4$ Nano-Crystallites via PVA Sol-Gel Route. *Journal of Alloys and Compounds*, **699**, 521-525. https://doi.org/10.1016/j.jallcom.2016.12.432

[3] Goldman, A. (2006) Modern Ferrite Technology. 2nd Edition, Springer Science and Business Media Inc., New York.

[4] Busca, G., Finocchio, E., Lorenzelli, V., Trombetta, M. and Rossini, S.A. (1996) IR

Study of Alkene Allylic Activation on Magnesium Ferrite and Alumina Catalysts. *Journal of the Chemical Society*, *Faraday Transactions*, **92**, 4687-4693. https://doi.org/10.1039/ft9969204687

[5] Candeia, R.A., Souza, M.A.F., Bernardi, M.I.B., Maestrelli, S.C., Santos, I.M.G., Souza, A.G. and Longo, E. (2006) $MgFe_2O_4$ Pigment Obtained at Low Temperature. *Materials Research Bulletin*, **41**, 183-190. https://doi.org/10.1016/j.materresbull.2005.07.019

[6] Abdel-Mohsen, F.F. and Emira, H.S. (2005) The Effect of Starting Materials and Preparation Process on the Properties of Magnesium Ferrite Pigment. *Pigment and Resin Technology*, **34**, 312-320. https://doi.org/10.1108/03699420510630327

[7] Shimizu, Y., Arai, H. and Seiyama, T. (1985) Theoretical Studies on the Impedance-Humidity Characteristics of Ceramic Humidity Sensors. *Sensors and Actuators*, **7**, 11-22. https://doi.org/10.1016/0250-6874(85)87002-5

[8] Liu, Y.L., Liu, Z.M., Yang, Y., Yang, H.F., Shen, G.L. and Yu, R.Q. (2005) Simple Synthesis of $MgFe_2O_4$ Nanoparticles as Gas Sensing Materials. *Sensors and Actuators B*: *Chemical*, **107**, 600-604. https://doi.org/10.1016/j.snb.2004.11.026

[9] Patil, J.Y., Mulla, I.S. and Suryavanshi, S.S. (2013) Gas Response Properties of Citrate Gel Synthesized Nanocrystalline $MgFe_2O_4$: Effect of Sintering Temperature. *Materials Research Bulletin*, **48**, 778-784. https://doi.org/10.1016/j.materresbull.2012.11.060

[10] Konishi, K., Maehara, T., Kamimori, T., Aono, H., Naohara, T., Kikkawa, H., Watanabe, Y. and Kawachi, K. (2004) Heating Ferrite Powder with AC Magnetic Field for Thermal Coagulation Therapy. *Journal of Magnetism and Magnetic Materials*, **272-276**, 2428-2429. https://doi.org/10.1016/j.jmmm.2003.12.591

[11] Tsunehiro, M., Kensuke, K., Tatsuo, K., Hiromichi, A., Takashi, N., Hiroyuki, K., Yuji, W. and Kanji, K. (2002) Heating of Ferrite Powder by an AC Magnetic Field for Local Hyperthermia. *Japanese Journal of Applied Physics*, **41**, 1620-1621. https://doi.org/10.1143/JJAP.41.1620

[12] Gateshki, M., Petkov, V., Pradhan, S.K. and Vogt, T. (2005) Structure of Nanocrystalline $MgFe_2O_4$ from X-Ray Diffraction, Rietveld and Atomic Pair Distribution Function Analysis. *Journal of Applied Crystallography*, **38**, 772-779. https://doi.org/10.1107/S0021889805024477

[13] Rabanal, M.E., Várez, A., Levenfeld, B. and Torralba, J.M. (2003) Magnetic Properties of Mg-Ferrite after Milling Process. *Journal of Materials Processing Technology*, **143-144**, 470-474. https://doi.org/10.1016/S0924-0136(03)00464-3

[14] Benko, F.A. and Koffyberg, F.P. (1986) The Effect of Defects on Some Photo Electrochemical Properties of Semiconducting $MgFe_2O_4$. *Materials Research Bulletin* **21**, 1183-1188. https://doi.org/10.1016/0025-5408(86)90045-0

[15] Reddy, P.V., Satyanarayana, R. and Seshagiri, Rao. T. (1984) Electrical Conduction in Magnesium Ferrite. *Journal of Materials Science Letters*, **3**, 847-849. https://doi.org/10.1007/BF00719568

[16] Sivakumar, N., Gnanakan, S.R.P., Karthikeyan, K., Amaresh, S., Yoon, W.S., Park, G.J. and Lee, Y.S. (2011) Nanostructured $MgFe_2O_4$ as Anode Materials for Lithium-Ion Batteries. *Journal of Alloys and Compounds*, **509**, 7038-7041. https://doi.org/10.1016/j.jallcom.2011.03.123

[17] Govha, J., Narasaiah, T.B., Kumar, P. and Shilpa, Ch. (2014) Synthesis of Nano-Magnesium Ferrite Spinel and Its Characterization. *International Journal of Engineering Research and Technology*, **3**, 1420-1422.

[18] Shakir, I., Sarfraz, M., Ali, Z.Z., Aboud, Z. and Agboola, P.O. (2016) Magnetically

Separable and Recyclable Graphene-$MgFe_2O_4$ Nanocomposites for Enhanced Photocatalytic Applications. *Journal of Alloys and Compounds*, **660**, 450-455. https://doi.org/10.1016/j.jallcom.2015.11.055

[19] Schulte, E.H. and Scoppa, P. (1987) Sources and Behavior of Technetium in the Environment. *Science of the Total Environment*, **64**, 163-179. https://doi.org/10.1016/0048-9697(87)90129-X

[20] Um, W. and Serne, R.J. (2005) Sorption and Transport Behavior of Radionuclides in the Proposed Low-Level Radioactive Waste Disposal Facility at the Hanford Site, Washington. *Radiochimica Acta*, **93**, 57-63. https://doi.org/10.1524/ract.93.1.57.58295

[21] Kesavamoorthi, R., Vigneshwaran, A.N., Sanyal, V. and Ramachandra, R.C. (2016) Synthesis and Characterization of Nickel Ferrite Nanoparticles by Sol-Gel Auto Combustion Method. *Journal of Chemical and Pharmaceutical Sciences*, **9**, 160-164.

[22] Yin, Y., Zhang, B., Zhang, X., Xu, J. and Yang, S. (2013) Nano $MgFe_2O_4$ Synthesized by Sol-Gel Auto-Combustion Method as Anode Materials for Lithium Ion Batteries. *Journal of Sol-Gel Science and Technology*, **66**, 540-543. https://doi.org/10.1007/s10971-013-2967-z

[23] Easwari, M. and Jesurani, S. (2017) Synthesis & Magnetic Properties of Magnesium Ferrite ($MgFe_2O_4$) Nanoparticles via Sol Gel Method. *International Research Journal of Engineering and Technology*, **9**, 110-113.

[24] Vijayakumar, G., Tamilarasan, R. and Dharmendirakumar, M. (2012) Adsorption, Kinetic, Equilibrium and Thermodynamic Studies on the Removal of Basic Dye Rhodamine-B from Aqueous Solution by the Use of Natural Adsorbent Perlite. *Journal of Materials and Environmental Science*, **3**, 157-170.

[25] Druc, A., Dumitrescu, A., Borhan, A., Nica, V., Iordan, A. and Palamaru, M. (2013) Optimization of Synthesis Conditions and the Study of Magnetic and Dielectric Properties for $MgFe_2O_4$ Ferrite. *Central European Journal of Chemistry*, **11**, 1330-1342.

[26] Jenkins, R. and Snyder, R.L. (1996) Introduction to X-Ray Powder Diffractometry. John Wiley & Sons, New York. https://doi.org/10.1002/9781118520994

[27] Ilhan, S., Izotova, S.G. and Komlev, A.A. (2015) Synthesis and Characterization of $MgFe_2O_4$ Nanoparticles Prepared by Hydrothermal Decomposition of Co-Precipitated Magnesium and Iron Hydroxides. *Ceramics International*, **41**, 577-585. https://doi.org/10.1016/j.ceramint.2014.08.106

[28] Hussein, S.I., Elkady, A.S., Rashad, M.M., Mostafa, A.G. and Megahid, R.M. (2015) Structural and Magnetic Properties of Magnesium Ferrite Nanoparticles Prepared via EDTA-Based Sol-Gel Reaction. *Journal of Magnetism and Magnetic Materials*, **379**, 9-15. https://doi.org/10.1016/j.jmmm.2014.11.079

[29] Naseri, M.G., Ara, M.H.M., Saion, E.B. and Shaari, A.H. (2014) Super Paramagnetic Magnesium Ferrite Nanoparticles Fabricated by a Simple, Thermal Treatment Method. *Journal of Magnetism and Magnetic Materials*, **350**, 141-147. https://doi.org/10.1016/j.jmmm.2013.08.032

[30] Park, D., Yun, Y.S. and Park, J.M. (2004) Reduction of Hexavalent Chromium with the Brown Seaweed Ecklonki Biomass. *Journal of Environmental Science and Technology*, **38**, 4860-4864. https://doi.org/10.1021/es035329+

[31] Holm, E., Gäfvert, T., Lindahl, P. and Roos, P. (2000) *In Situ* Sorption of Technetium Using Activated Carbon. *Applied Radiation and Isotopes*, **53**, 153-157. https://doi.org/10.1016/S0969-8043(00)00127-5

[32] Saad, A.K., Rehman, R. and Khan, M.A. (1994) Sorption of Cesium on Bentonite.

Waste Management, **14**, 629-642. https://doi.org/10.1016/0956-053X(94)90035-3

[33] Ali, R.M., Hamad, H.A., Hussein, M.M. and Malash, G.F. (2016) Potential of Using Green Adsorbent of Heavy Metal Removal from Aqueous Solutions: Adsorption Kinetics, Isotherm, Thermodynamic, Mechanism and Economic Analysis. *Journal of Ecological Engineering*, **91**, 17-332. https://doi.org/10.1016/j.ecoleng.2016.03.015

[34] Reddad, Z., Gerente, C., Andres, Y. and Cloirec, L.P. (2002) Adsorption of Several Metal Ions onto a Low-Cost Biosorbent: Kinetic and Equilibrium Studies. *Journal of Environmental Science and Technology*, **36**, 2067-2073. https://doi.org/10.1021/es0102989

[35] Hu, D. and Wang, L. (2016) Adsorption of Amoxicillin onto Quaternized Cellulose from Flax Noil: Kinetic, Equilibrium and Thermodynamic Study. *Journal of the Taiwan Institute of Chemical Engineers*, **64**, 227-234. https://doi.org/10.1016/j.jtice.2016.04.028

[36] Langmuir, I. (1918) The Adsorption of Gases on Plane Surfaces of Glass, Mica and Platinum. *Journal of the American Chemical Society*, **40**, 1361-1403. https://doi.org/10.1021/ja02242a004

[37] Freundlich, H.M.F. (1906) Über die adsorption in Lösungen. *Industrial & Engineering Chemistry Fundamentals*, **57**, 385-470.

[38] Gokila, S., Gomathi, T., Sudha, P.N. and Sukumaran, A. (2017) Removal of the Heavy Metal Ion Chromiuim (VI) Using Chitosan and Alginate Nanocomposites. *International Journal of Biological Macromolecules*, **104**, 1459-1468. https://doi.org/10.1016/j.ijbiomac.2017.05.117

[39] Ben Tahar, L., Habid, O.M. and Jaipallah, A.A.M. (2017) Synthesis of Magnetite Derivatives Nanoparticles and Their Application for the Removal of Chromium (VI) from Aqueous Solutions. *Journal of Colloid and Interface Science*, **512**, 115-126. https://doi.org/10.1016/j.jcis.2017.10.044

[40] Dubey, S., Gusain, D. and Sharma, Y.C. (2016) Kinetic and Isotherm Parameter Determination for the Removal of Chromium from Aqueous Solutions by Nano-Alumina, a Nano-Adsorbent. *Journal of Molecular Liquids*, **219**, 1-8. https://doi.org/10.1016/j.molliq.2016.01.021

[41] Xiao, Z., Zhang, H., Xu, Y., Yuan, M., Jing, X., Huang, J., Li, Q. and Sun, D. (2017) Ultra-Efficient Removal of Chromium from Aqueous Medium by Biogenic Iron-Based Nanoparticles. *Separation and Purification Technology*, **174**, 466-473. https://doi.org/10.1016/j.seppur.2016.10.047

[42] Qiu, H., Lv, L., Pan, B., Zhang, Q., Zhang, W. and Zhang, Q. (2009) Critical Review in Adsorption Kinetic Models. *Journal of Zhejiang University Science B*, **10**, 716-724. https://doi.org/10.1631/jzus.A0820524

[43] Qiu, W., Yang, D., Xu, J., Hong, B., Jin, H., Jin, D., Peng, X., Li, J., Ge, H. and Wang, X. (2016) Efficient Removal of Cr(VI) by Magnetically Separable $CoFe_2O_4$/Activated Carbon Composite. *Journal of Alloys and Compounds*, **678**, 179-184. https://doi.org/10.1016/j.jallcom.2016.03.304

[44] Venkatesha, T.G., Viswanatha, R., Nayaka, Y.A. and Chethana, B.K. (2012) Kinetics and Thermodynamics of Reactive and Vat Dyes Adsorption on MgO Nanoparticles. *Chemical Engineering Journal*, **198**, 1-10.